Article

New ICT-Based Ratiometric Two-Photon near Infrared Probe for Imaging Tyrosinase in Living Cells, Tissues, and Whole Organisms

Javier Valverde-Pozo [1], Jose Manuel Paredes [1,*] , Maria Eugenia García-Rubiño [1], Thomas J. Widmann [2] , Carmen Griñan-Lison [2,3,4] , Silvia Lobon-Moles [1], Juan Antonio Marchal [3,5,6] , Jose Maria Alvarez-Pez [1] and Eva Maria Talavera [1,*]

[1] Nanoscopy-UGR Laboratory, Department of Physical Chemistry, Faculty of Pharmacy, Unidad de Excelencia en Quimica Aplicada a Biomedicina y Medioambiente (UEQ), University of Granada, C. U. Cartuja, 18071 Granada, Spain
[2] GENYO, Centre for Genomics and Oncological Research, Pfizer/University of Granada/Andalusian Regional Government, 18016 Granada, Spain
[3] Instituto de Investigación Biosanitaria (ibs.GRANADA), 18012 Granada, Spain
[4] UGC de Oncología Médica, Complejo Hospitalario de Jaen, 23007 Jaen, Spain
[5] Centre for Biomedical Research (CIBM), Biopathology and Regenerative Medicine Institute (IBIMER), University of Granada, 18100 Granada, Spain
[6] Department of Human Anatomy and Embryology, Faculty of Medicine, University of Granada, 18016 Granada, Spain
*   Correspondence: jmparedes@ugr.es (J.M.P.); etalaver@ugr.es (E.M.T.); Tel.: +34-958243829 (J.M.P.); +34-958243828 (E.M.T.)

Abstract: Melanoma is a type of highly malignant and metastatic skin cancer. In situ molecular imaging of endogenous levels of the melanoma biomarker tyrosinase (TYR) may decrease the likelihood of mortality. In this study, we proposed the weakly fluorescent probe 1-(4-(2-(4-(dicyanomethylene)-4H-chromen-2-yl)vinyl)phenyl)-3-(4-hydroxybenzyl)urea (DCM-HBU), which releases a strong red-shifted fluorescent signal after a TYR-mediated oxidation followed by hydrolysis of the urea linkage. The large Stokes shift of the dye is owed to the recovery of the intramolecular charge transfer (ICT) effect. The resulting probe derivate shows a highly ratiometric fluorescence output. Furthermore, the simultaneous excitation by two near-infrared (NIR) photons of the released derivative of dicyanomethylene-4H-pyran (DCM-NH$_2$) fluorophore could avoid the usual drawbacks, such as cellular absorption, autofluorescence, and light scattering, due to an usually short wavelength of the excitation light on biological systems, resulting in images with deeper tissue penetration. In addition, the probe is useful for the quantitative sensing of TYR activity in vivo, as demonstrated in zebrafish larvae. This new ratiometric two-photon NIR fluorescent probe is expected to be useful for the accurate detection of TYR in complex biosystems at greater depths than other one-photon excited fluorescent probes.

Keywords: tyrosinase; NIR sensor; two-photon excitation; melanoma; zebrafish; bioimaging

1. Introduction

The biological and clinical importance of having readouts of the biological activity of enzymes in physiological and disease conditions, along with the possibility of non-invasive detection of their activities, high spatial resolution, and great sensitivity, makes the use of fluorescent probes that penetrate inside living cells, one of the main options for detecting enzymatic activity in vivo [1–3].

To achieve real-time in situ imaging of enzymes in living cells, tissues, and whole organisms, fluorescent substrates must interact with the enzyme, leading to a change in its fluorescence that allows enzyme activity to be detected. Among the fluorescent methods

fluorescence microscopy is extensively used in estimating enzyme activities [4–6], drug distribution monitoring [7], image-guided surgery [8], preclinical research, and clinical diagnosis and therapy [9–11]. However, the most prominent enzymatic probes utilize one-photon microscopy (OPM), which requires UV−V, which is light excitation that, due to its short wavelength, results in limited in vivo depth penetration, cellular autofluorescence, and light scattering [12]. To avoid these drawbacks, a technique can be used that consists in the excitation of the fluorophore by means of two simultaneous photons of a wavelength that doubles or exceeds that needed to excite the same fluorophore with a single photon [13–15]. Two-photon microscopy (TPM) was predicted by Nobel laureate Maria Goeppert Mayer in 1931 [16] and was applied by Webb in a cellular environment in 1990 [17]. TPM uses NIR photons as the excitation source of the fluorophores, resulting in images of deeper layers in biological systems. Moreover, it is suitable for in vivo enzyme activity studies with three-dimensional resolution, so that TPM gains immense support for clinical optical imaging applications [18] as DNA intercalators for visualization of nuclei in live cells [19], probes based on carbon dots (pH-CDs) for the monitoring of pH in cells, tissue, and zebrafish [20], sensing endoplasmic reticulum (ER) peroxynitrite in Parkinson's disease models [21] or detection of glutathione (GSH) in living cells, mice models, and clinical specimens [22].

In addition to being excitable by two simultaneous photons, the probes should be ratiometric, as was extensively researched and reflected in several excellent reviews on this topic [23–26]. The quantification of an analyte using fluorescent probes emitting only one signal can be very inaccurate, since several factors independent of the analyte, such as the microenvironment around the probe, its local concentration, photobleaching, or certain instrumental parameters, interfere with correct analysis. In contrast, ratiometric fluorescent probes are based on analyte-induced changes in the intensity of two emission bands. Thus, the ratio of intensities at two wavelengths correlates directly with the concentration of the analyte providing self-calibration and correcting the analyte-independent factors listed above. Two-photon ratiometric probes demonstrate excellent performances in target biosensing, bioimaging, and biomedicine applications in vitro and in vivo [26].

Tyrosinase (TYR), also called monophenol monooxygenase, is a cuproprotein with two copper ions in the active site, both of which are coordinated by three histidine residues (type-3 copper proteins). It catalyzes the conversion of monophenols to *ortho*-quinones via *ortho*-diphenols. TYR catalyzes the first two steps in mammalian melanogenesis, initiating melanin formation by tyrosine oxidation [27,28]. Although melanin primarily has a photoprotective function in human skin, the accumulation of increased amounts of melanin in specific parts of the skin results in undesirable freckles and brown spots on the human body. Additionally, it is the cause of enzymatic browning in fruits and fungi, which has a great visual impact that decreases the commercial quality and value of the products [29]. However, even more important for human health is the abnormal expression or activation of TYR, since it is associated with several disorders, such as melanoma and Parkinson's disease. Therefore, monitoring the TYR activity will help accurate diagnosis and treatment of these illnesses [30].

The traditional colorimetric method to detect TYR activity shows very low sensitivity [31], and was initially replaced by other methods based on electrochemistry [32,33] and quantum dots luminescence [34]. Fluorescence spectroscopy is also used to design highly sensitive TYR probes. Thus, an oligo (phenylenevinylene) containing a tyrosine moiety was synthesized as an "on/off" fluorescent probe to detect TYR activity by oxidation of tyrosine to quinone, which quenched fluorescence [35]. A fluorescent NIR probe that incorporates tyramine (a TYR substrate) into the cyanine structure was developed by Wolfbeis' group [36]. Reaction with TYR in the presence of oxygen forms a quinone that quenches the fluorescence of the probe. However, to achieve high-sensitivity bioimaging in living systems by fluorescence microscopy, the most suitable approach is to develop a TYR off/on sensor. In this sense, Wu et al. [37] incorporated the 3-hydroxybenzyl recognition moiety into a fluorescent reporter to facilitate hydroxylation by TYR at the 4-position, and then

from enzymatic oxidation to orthoquinone, which in turn undergoes a rapid intramolecular electron rearrangement that initiates cleavage of orthoquinone. In this way, it is possible to eliminate the interference from reactive oxygen species.

With these ideas in mind and taking into account that a widely used strategy for obtaining ratiometric fluorescent probes is the use of molecules with electron-donor electron-acceptor (D-A) ability giving rise to an intramolecular charge transfer complex (ICT). To develop ICT based probes, there are different types of backbones used, the most common includes donor–π–acceptor (D–π–A) dipoles, D–π–D, and D–π–A–π–D quadrupoles and two-dimensional octupoles [38–40]. Some common examples of these structures are represented in Figure S1 in the Supplementary Materials. Some common advantages of ICT-based probes are the long Stokes shifts and the possibility to tune the optical properties [41]. In this work, we developed a dicyanomethylene-4H-pyran (DCM)-based [42] fluorescence off/on probe. The overall design strategy of the probe DCM-HBU was founded on the attachment of an enzyme active moiety 4-hydroxybenzylamine (very similar to tyrosine) to a signal reporter NIR TP DCM, perturbing the ICT effect that controls the spectral properties of DCM [43]. By treatment with TYR, its catalytic action restores the ICT process and concomitantly the fluorescence of the DCM-NH$_2$ [44], providing a ratiometric signal between the emission maxima from the dye and the probe. Due to the enzymatic reaction, color changes from yellow to red, allowing colorimetric detection of TYR with the naked eye. Moreover, this fluorescent probe can be excited by two simultaneous NIR photons. This new probe was successfully applied to the detection of TYR in solution, in living cells, tissues, and in whole organisms in vivo, using zebrafish. To the best of our knowledge, this is the first report of a ratiometric two-photon small-molecular NIR probe for the bioimaging of TYR in vitro/vivo.

2. Materials and Methods

2.1. Reagents and Standards

All starting materials (reagents and solvents) were purchased from Sigma-Aldrich (Madrid, Spain), including the enzymes TYR, dipeptidyl peptidase IV (DPP IV), acetyl-cholinesterase (AChE), lipase (PNLIP), and the enzyme inhibitor quercetin, with the highest degree of purity. Alanine aminopeptidase (ANEP) was produced and purified as previously described [44].

2.2. Sample Preparation

The 0.5 mM and 2.9 mM stock solutions of DCM-NH$_2$ and DCM-HBU, respectively, were prepared in deuterated DMSO for purity testing by nuclear magnetic resonance. The experiments were carried out in PBS/DMSO buffer solution (7/3, *v/v*).

2.3. Instrumentation

UV-visible absorption spectra were collected using a Lambda 650 UV-visible spectrophotometer (PerkinElmer, Waltham, MA, USA). Steady-state fluorescence and kinetics were measured by a Jasco FP-8300 spectrofluorometer (Jasco, Tokyo, Japan). Spectrophotometry and spectrofluorimetry were performed using a temperature controller.

One-photon microscopy images were acquired with an Abberior scanning microscope (Abberior Instruments GmbH, Göttingen, Germany) using a pulsed excitation laser (485 nm, 40 MHz) and an objective UPlanSApo (1.4 NA, 100X) oil immersion. The pinhole size was set to 1 Airy unit (AU) in every measurement. Two-photon microcopy images were obtained with a confocal MicroTime 200 fluorescence microscope system (PicoQuant GmbH, Berlin, Germany). The excitation source was a Chameleon Discovery NX tunable laser (Coherent Laser Group, Santa Clara, CA, USA). The intensity of the laser was controlled using a set of polarizers. Later, the excitation beam passed through an achromatic quarter-wave filter (AQWP05-M-600, Thorlabs, Jessup, MD, USA) and by an F73-705SG dichroic mirror (AHF/Chroma, Tübingen, Germany) to direct the beam to an inverted microscope system (IX-71, Olympus, Tokyo, Japan) with an oil immersion

objective (1.4 NA, 100X). Fluorescence emission was acquired with a 500 nm longpass filter (AHF/Chroma, Tübingen, Germany) and directed to a 75 μm pinhole. Later, a 600 DCXR dichroic beam splitter (AHF/Chroma) separated the emission into two detection channels (red and green). The red channel used bandpass filters, 685/70 (Semrock/AHF), and the green channel a 520/35 filter (Semrock/AHF). The detectors used were two different single-photon avalanche diodes (SPCM-AQR 14, PerkinElmer, Waltham, MA, USA).

Images of zebrafish embryos were performed on a Nikon SMZ18 fluorescent stereo microscope with a color DS-Ri2 digital camera (16.25 Mpx) using filter settings for red fluorescent protein (RFP).

2.4. Image Processing

Images from two channels were exported separately as matrix data and analyzed using *Fiji Is Just ImageJ* v1.53t [45]. In the image analysis, we performed a Gaussian filter (sigma = 2) to the raw images. Later, we manually selected the regions of interest (ROI) through a threshold based on the intensity. Outside the ROI, a not a number (NaN) was assigned to pixels. These images were used to calculate the ratio value dividing both segmented channels (red and green) pixel to pixel.

2.5. Cell Culture

The human melanoma primary patient-derived cell line Mel-1 comes from a malignant metastatic melanoma (stage M1a) skin biopsy and was provided by the Biobank of the Andalusian Public Health System (Spain); A-375 melanoma cell line was obtained from American Type Culture Collection (ATCC). All cell lines were cultured in Dulbecco's Modified Eagle Medium (DMEM; Sigma-Aldrich, St Louis, MO, USA) supplemented with 10% heat-inactivated fetal bovine serum (FBS) (BioWhittaker; Lonza, Basel, Switzerland), 1% L-glutamine, 2.7% sodium bicarbonate, 1% Hepes buffer, and with 1% of a solution of penicillin/streptomycin (10,000 U mL^{-1} penicillin G and 10 mg mL^{-1} streptomycin; Sigma-Aldrich, St Louis, MO, USA) and they were maintained at 37 °C in an atmosphere containing 5% CO_2. In order to carry out the microscopy experiments, cells were seeded onto μ-slide 8-well IbiTreat plates at a density of 5–11 × 10^4 cells/well and then the samples were washed three times using phosphate buffered saline (PBS) 1× and bathed into DMEM buffer with 5 × 10^{-6} M of DCM-HBU.

2.6. Generation of Tumours

In order to create subcutaneous xenograft tumours, an eight-week-old male NODSCID gamma mouse (NOD. Cg-Prkdcscid Il2rgtm1 Wjl/SzJ, NSG) was employed. Each procedure was authorized by the Institutional Animal Care and Use Committee of the University of Granada (ethical code: 03/07/2017/086). Mice were controlled at 20–24 °C, 50% relative humidity (RH), and a 10:14 h light:dark cycle with food and water provided ad libitum. A human skin cancer cell line, A-375, was employed to generate subcutaneous xenograft tumours by injecting 1 × 10^6 cells in 0.05 mL Matrigel and 0.05 mL Roswell Park Memorial Institute (RPMI) medium using 26-gauge needles. When the tumour reached 300 mm^3, the mouse was euthanized by cervical dislocation. For TPM analysis, tumours were excised, fixed in 4% paraformaldehyde (PFA), embedded in optimal cutting temperature (OCT) compound, and selected using a cryotome at 10 mm thickness for further analysis.

2.7. Zebrafish

Zebrafish (*Danio rerio*) were kept at the fish facility, CIC, University of Granada, Spain, in fish tanks with constant water flow at 28.5 °C, following maintenance and breeding recommendations from the zebrafish handbook "https://zfin.org/zf_info/zfbook/zfbk.html (accessed on 1 February 2023)" and according to the European Directive 2010/63/EU assuring animal welfare. For egg lay, wild-type males and females were set up in a breeding tank. Egg lay occurred shortly after the onset of light in the morning of the following day. Embryos were raised in E3 embryo medium (5 mM NaCl, 0.17 mM KCl, 0.33 mM $CaCl_2$,

0.33 mM MgSO$_4$, and 10^{-5}% Methylene Blue) at 28.5 °C until the desired stage. Embryos of the desired stage were incubated in E3 medium with 10 μM DCM-HBU (1:288 of stock solution at 2.9 mM in DMSO) for 3 h and then shortly washed with fresh E3 medium. For inhibition of the DCM-HBU processing tyrosine kinase, embryos were incubated with 200 μM quercetin (1:50 of stock 10 mM) for 3 h prior to adding 10 μM DCM-HBU for 3 h. Controls were incubated in E3 medium with DMSO (1:50) for 6 h. Subsequently, anesthetized (0.1 to 0.15 mg mL^{-1} MS222) live embryos were imaged. Overlay images and quantification of red fluorescence intensity were carried out with *Fiji Is Just ImageJ* [45].

3. Results

3.1. Synthesis

Synthesis of DCM-HBU was accomplished through a one-step route starting from ICT derivative DCM-NH$_2$, which was prepared as previously described by Sun et al. [46] (see synthetic route in Scheme S1, Supplementary Materials). The reaction of the aniline derivative with 4-hydroxybenzylamine provided the corresponding amide to obtain DCM-HBU, (Scheme 1). The final product was characterized by ^{1}H nuclear magnetic resonance (NMR) and time-of-flight mass spectrometry (TOF MS) and IR (see the Supplementary Materials for more details on the synthesis and characterization).
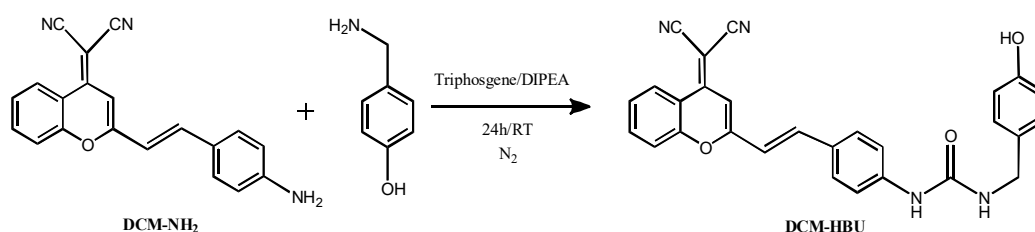
Scheme 1. Synthetic route of DCM-HBU (compound **2**).

3.2. Photophysical Characterization of the Enzymatic Reaction

Firstly, we recorded the absorption (Figure 1a) and emission (Figure 1b) spectra of DCM-NH$_2$ in six different solvents. ICT causes a red shift in fluorescence and is linked to the increase in dipole moment upon excitation [47]. The fluorescence lifetime was also calculated in a great number of solvents, in most of them, a biexponential analysis was necessary to fit the decay traces. From the results of these data, two lifetimes were found and attributable to cis and trans isomer fluorescence. However, in DMSO, the decay traces were well-fitted using a monoexponential function, and a fluorescence lifetime of 2.25 ns, higher than in other solvents, was obtained [48], hence the DCM fluorescence decay dissolved in DMSO must be attributed to a relaxed fluorescent state. From both, previous works and our results [44,48], DMSO appears to be the best solvent for DCM in view of its longer fluorescence decay time and low photoisomerization efficiency. As a conclusion, the presence of a certain amount of DMSO in the solvent used for fluorescence studies is justified. In our previous studies using PBS buffer, the fluorescence signals decreased when less than 30% DMSO was used, along with a rapid precipitation of the dye after dissolution [44].
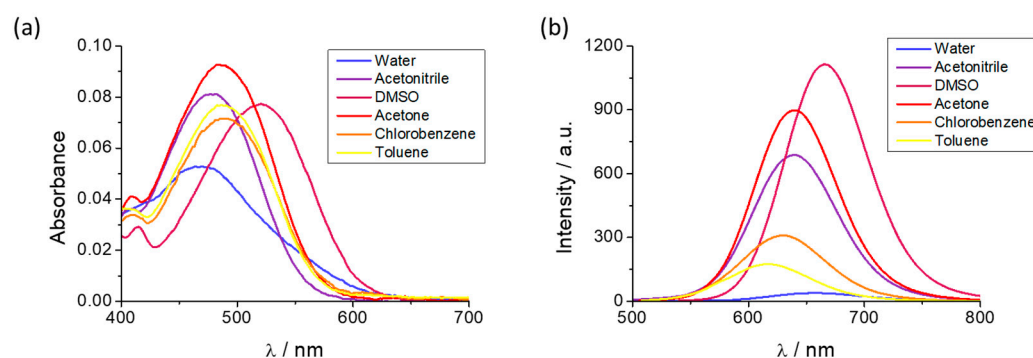
Figure 1. (**a**) Absorption spectra of the compound DCM-NH$_2$, 1.7 μM in different solvents. (**b**) Emission spectra of the compound DCM-NH$_2$, 1.7 μM in different solvents.

The absorption and emission spectra profiles of DCM–NH$_2$ and DCM-HBU in the PBS/DMSO (7/3, *v*/*v*), pH = 7.4 solution are shown in Figure 2. The DCM-NH$_2$ spectrum shows an ICT absorption band around 480 nm (ε = 37,685 L mol^{-1} cm^{-1}) in accordance with the values provided elsewhere [44], while the band from DCM-HBU has an absorption maximum at 453 nm (ε = 5409 L mol^{-1} cm^{-1}; see Figures S2 and S3). Correspondingly, the emission spectrum of DCM-HBU (Figure 2 and Figure S4) shows (at λ_{ex} = 453 nm) an emission band with its maximum around 570 nm (Φ = 7.71%), and the DCM-NH$_2$ spectrum (at λ_{ex} = 480 nm) (Figure S5) shows an intense emission band with its maximum at 662 nm (Φ = 16.92%) (Figure S6). Fluorescence quantum yields, absorptivity coefficients, and Stokes shift of DCM-NH$_2$ of the rest of solvents used in this work are summarized in Table S1 in Supplementary Materials, and absorption and emission spectra. The fluorescence lifetimes of DCM-NH$_2$ and DCM-HBU were 227.3 and 554.4 ps, respectively (Figure S7). On the other hand, we evaluated the pH sensitivity of the compound DCM-NH$_2$. Our results show a maintenance on the intensity in the range of pH measured (Figure S8). Finally, to complete the photophysical characterization, we checked the resistance to photobleaching of both compounds. The samples were continuously radiated and the intensity in the maxima wavelength of emission was registered. After 30 min of radiation, we detected a decrease of 5% and 10% in the intensity of DCM-HBU and DCM-NH$_2$, respectively (Figure S9).
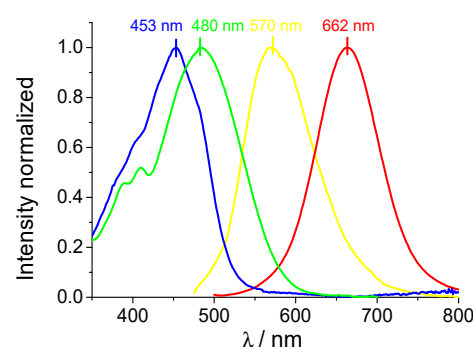

Figure 2. Normalized absorption spectra of the pure compounds DCM-HBU (blue line) and DCM−NH$_2$ (green line); normalized emission spectra of the pure compounds DCM-HBU (yellow line) and DCM-NH$_2$ (red line) by excitation at 453 nm and 480 nm, respectively.

The addition of TYR (0.13 mg mL^{-1}) to the DCM-HBU in PBS/DMSO (7/3, *v*/*v*), 25 μM, and pH = 7.4 solution resulted in a decrease in the emission band with λ_{max} = 570 nm (λ_{ex} = 453 nm) corresponding to the probe, along with a concomitant increase in the emission band attributed to DCM-NH$_2$ (Figure 3a). The kinetics were followed every minute for 2 h at 37 °C (see Figure S10). As can be observed, the new emission band that appears after adding the enzyme is assigned to that one shown by free DCM-NH$_2$. The ratio I$_{662}$/I$_{570}$ between these two fluorescence signals achieves a four-times increase due to the addition

of TYR after 100 min, remaining constant after this time (Figure 3b). Furthermore, we tested the activity of the enzyme at different pH values and temperatures (Figure S11), demonstrating that the best catalytic activity is at approximately pH 7.5 and 37 °C.
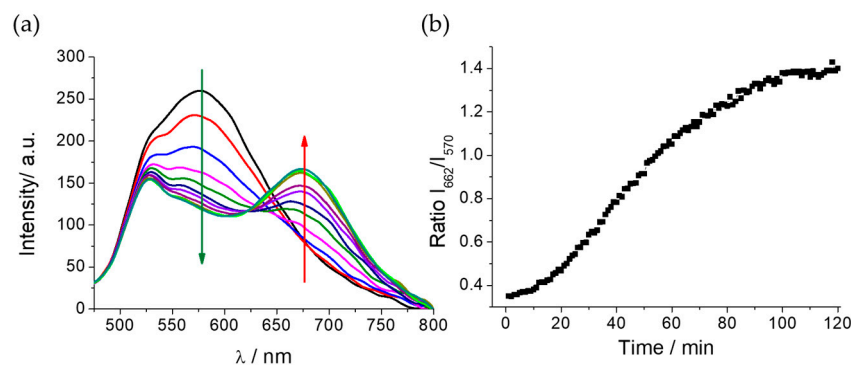

Figure 3. (**a**) Evolution of the emission spectra of DCM-HBU (25 μM) with TYR (0.13 mg mL^{-1}) observed every 10 min for 2 h by excitation at 450 nm at 37 °C; and (**b**) Ratiometric measurements of fluorescence signals of I_{662}/I_{570} at different times.

3.3. Proposed Mechanism for TYR Response

According to the reaction mechanism of the tyrosinase catalysis proposed by Ma et al. [37], the Scheme 2 shows the necessary steps for sensing TYR by the new probe DCM-HBU. As further test of the proposed mechanism, the IR spectra of the dye and the probe (both dissolved in DMSO) along with a sample of the reaction mixture after 2 h reacting (PBS/DMSO as solvent) were recorded and are shown in Figure S12. Among the most prominent signals in the spectrum from the reaction sample are the intense band in the region of hydrogen tension due to solvent water and a band of medium intensity assignable to the presence of C = O groups that is consistent with the presence of ketones.
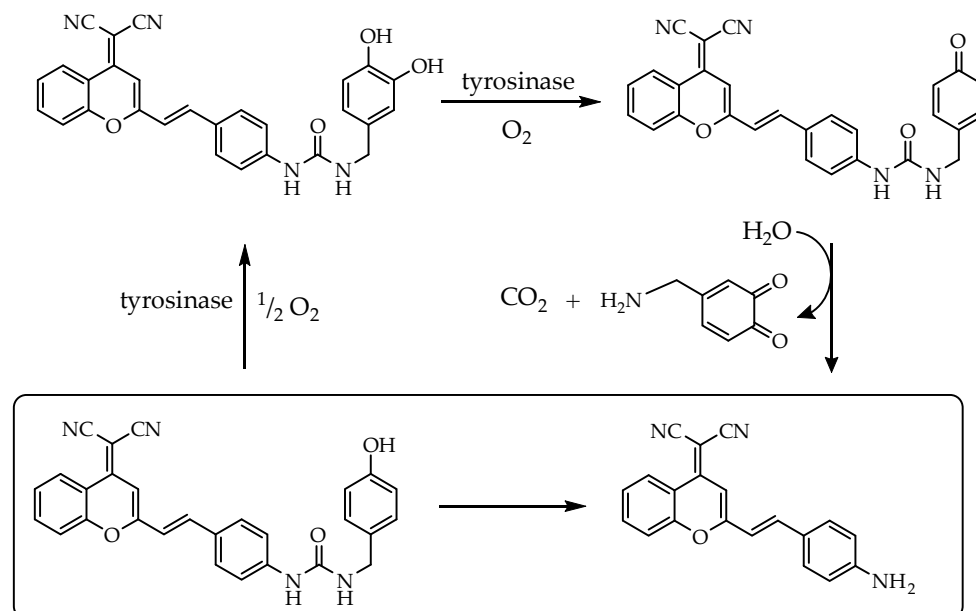
Scheme 2. Proposed sensing mechanism of DCM-NH$_2$ release by TYR.

3.4. Sensitivity of the Probe towards TYR

To show unambiguously that DCM-HBU senses only TYR, we investigated the specificity of the probe. In Figure 4, the fluorescence I_{662}/I_{570} ratio of the DCM-HBU in the presence of TYR is compared to the same fluorescence ratio recorded when the probe

was incubated in the presence of other related enzymes, such as ANEP, DPP IV, AChE, and PNLIP. The results demonstrate the very high specificity of DCM-HBU towards the enzymatic action of TYR.
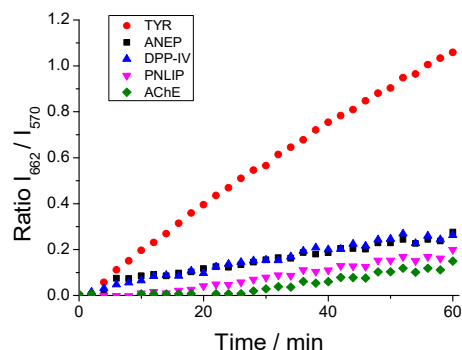

Figure 4. Ratiometric measurements of fluorescence signals of I_{662}/I_{570} of DCM-HBU (10 μM) over time in the presence of different related enzymes at the same concentration (5 μg mL^{-1}) by excitation at 450 nm at 37 °C.

3.5. Ratiometric Monitoring of TYR Activity in Tumour Cells and Tissues

After photophysical characterization in solution, the study was carried out on tumour cells by single-photon excitation microscopy. Moreover, we measured the TYR activity in melanoma cells and in ex vivo tissues under two-photon excitation. In order to show the two-photon absorption properties of the probe, we measured the fluorescence emission of the compounds DCM-NH$_2$ and DCM-HBU at different wavelengths of excitation. Figure S13 shows the normalized intensity by the excitation power in the range of 720–1000 nm. Our results show a maxima emission of both compounds under an excitation of 800 nm. Next, to confirm the two-photon absorption properties, we measured the fluorescence intensity of DCM-NH$_2$ and DCM-HBU at different input power. The representations of the logarithmic plot of the power dependence of the relative two-photon induced fluorescence intensity are shown in Figure S14. The linear fits of these data displayed slopes of 2.01 ± 0.11 and 2.32 ± 0.21, confirming the two-photon excitation process in both compounds.

As a model of melanoma, we selected MEL1 (a primary cell line) and A-375 (a well-established cell line). Firstly, we performed a study to confirm that our probe is sensitive to intracellular TYR enzymatic activity. For this purpose, images of both cell lines were collected for 30 min after adding DCM-HBU (5 μM) in PBS/DMSO (7/3, *v/v*). The results reveal that in both cell lines red fluorescence increases over time, while green fluorescence remains almost constant, which leads to a progressive increase in the value of the image ratio (Figure S15). This increase is very likely to be caused by the release of the DCM-NH$_2$ product due to the action of the tyrosinase enzyme on the probe. Interestingly, we observed a faster increase in the ratio values of MEL1 versus A-375 cells. This fact suggests a higher enzymatic activity in this human primary cell line (Figure S16).

In order to demonstrate that the increase in NIR emission and, consequently, in the ratio values, is mainly due to TYR enzymatic activity, MEL1 was also measured under the same previous conditions but in the presence of the TYR inhibitor quercetin [49,50] (Figure 5a). The ratio values were plotted as a function of time for both cells without quercetin and those exposed to the inhibitor (Figure 5b), in which a great increase in the fluorescent signal in the red channel is clearly observed when the inhibitor is absent, while in the presence of quercetin, the enzymatic reaction is virtually inhibited. This experiment confirms that in this cell line, TYR is mainly responsible for the conversion of the DCM-HBU probe to DCM-NH$_2$.
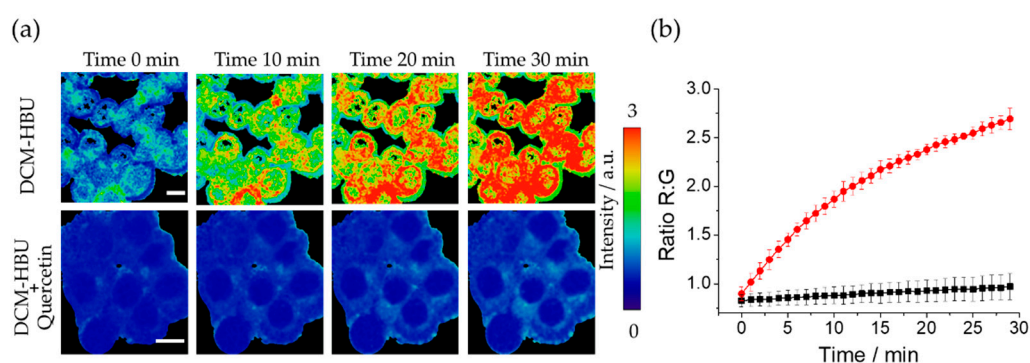
Figure 5. (**a**) R:G ratio maps of live MEL1 cell line at different time points after adding DCM-HBU (5 μM) without (upper panel) and with (lower panel) the TYR inhibitor quercetin (100 μM) (λ_{ex} = 453 nm). The scale bars represent 10 μm; (**b**) representation of the R:G ratios from microscopy images in absence (circles) and presence (square) of quercetin. Error bars represent the standard deviation (SD).

Next, in order to confirm the probe's ability to be excited by two photons that double or exceed the wavelength of excitation of the same fluorophore with a single photon, the A-375 cell line was excited with a wavelength of 800 nm. Figure 6a shows representative two-photon excitation images obtained, where an increase in the R:G ratio value after 10 min of incubation can be observed. The kinetics of the R:G ratio increase is shown in Figure 6b and Video S1, representing R:G ratio values versus time. The results show an increase in the ratio values during the first 10 min of incubation. In Figure 6c, fluorescence lifetime imaging microscopy (FLIM) of the fluorophore revealed on live A-375 cells that the dye has a longer lifetime (above 1.2 ns) in the cell periphery, compatible with its presence at the cytoplasmic membrane, one of the cellular structures with higher lipophilia. However, the greater polarity of other structures in the cytoplasm causes a faster deexcitation that corresponds to a lower fluorescence lifetime (around 0.9 ns). The fluorescence lifetime of DCM-NH$_2$ was previously studied in different solvents [44], and although the changes in its fluorescence lifetime can be caused by polarity differences in the probe's microenvironment, more experiments should be performed to determine if additional causes exit. The images obtained also show the typical accumulation pattern of DCM-NH$_2$ in cells, mainly in lysosomes, as previously was indicated [51]. The pattern of accumulation, as well as the difference in fluorescence lifetime in the different structures of DCM-NH$_2$, are promising behaviors to perform deeper fluorescence lifetime imaging studies of organelle isolation and internal lipophilia through changes in the fluorescence lifetime.

As we mentioned, the potential use in two-photon excitation is the key for its employment in more complex biological structures, including tissues or even in whole body animals. In this context, our first approach was to detect the enzyme TYR in tissues through the sensor. For this purpose, we selected A-375-derived tumours as a model of human melanoma for the study. The use of an excitation wavelength of 800 nm lowers autofluorescence to nearly undetectable levels (see Figure S17), a fundamental advantage in the ratiometric-based sensors.

We incubated these tissues with a solution of DCM-HBU (5 μM), and measured the green and NIR emission at four time points (initial time, 1, 3 and 14 h). From this data we calculated the ratio images (see Figure 7a) at different z positions that also allowed us to reconstruct 3D images (see Figure 7b and Video S2). Once the compound was added, the NIR fluorescence intensity increased over time, translated to ratio value, reaching its maximum value at 14 h (Figure 7c). On the other hand, green fluorescence, remained almost constant without significant changes (see Figures S17 and S18). This resulted in an increase in the value of the R:G ratio from 0.8 to 2.5, as can be seen in the Figure 7c. It follows, therefore, that the activity of the enzyme TYR causes the cleavage of the DCM-HBU sensor, releasing the DCM-NH$_2$ product, which is responsible for the NIR fluorescence.
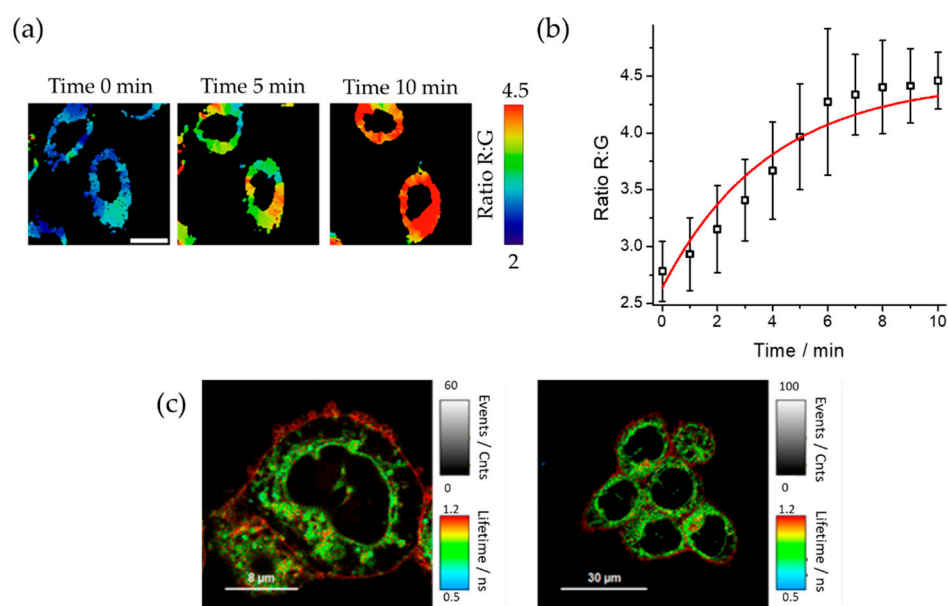
Figure 6. (**a**) Fluorescence microscopy R:G ratio maps of the live A-375 cell line at different time points after adding DCM-HBU obtained by two-photon excitation at 800 nm (G: 520/35, R: 685/70). Scale bar represents 10 μm; (**b**) representation of the R:G ratios from microscopy images. Error bars represent the SD; and (**c**) FLIM of live A-375 cell line after adding DCM−NH$_2$ 5 μM by excitation with two 800 nm photons.
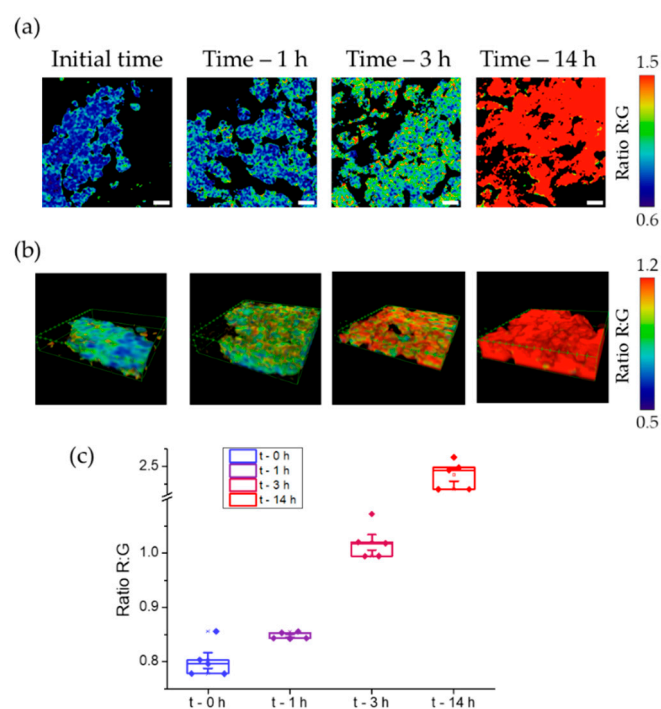

Figure 7. (**a**) Ratiometric images of A-375 tumours after adding DCM-HBU (5 μM) over time using two-photon microscopy with excitation at 800 nm. Scale bars are 10 μm. (**b**) 3D ratiometric images of A-375 tumours using two-photon microscopy with excitation at 800 nm. (**c**) Representation of the R:G ratio values from microscopy images. Boxes represent the 25th, 50th, and 75th percentiles. Whiskers represent the SE.

3.6. In Vivo Imaging of TYR in Zebrafish

In a recent study, TYR activity was found in zebrafish larvae; however, its activity was determined only qualitatively [37]. Here, we went further and we completed, for the first time to our knowledge, a deeper study quantifying the differences in TYR activity in vivo in zebrafish larvae and embryos at different days post fertilization (dpf) in the absence or presence of an inhibitor (quercetin).

Zebrafish embryos and larvae of different dpf, when incubated with the DCM-HBU probe, show the characteristic NIR fluorescence indicating the release of the DCM-NH$_2$ compound due to the action of the TYR enzyme in yolk sac and larval tissues (Figure 8a). Both the eye and the central nervous system (CNS) are the tissues where most enzymatic activity is observed, while skin and muscles do not show strong NIR fluorescence. Control zebrafish incubated with DMSO display a low level of autofluorescence (Figure S20). In order to demonstrate that the NIR fluorescence observed with DCM-HBU is due to the action of the TYR enzyme, a co-inhibition study was performed at every time point. In the presence of the known TYR inhibitor quercetin [49,50], DCM-HBU was not processed to DCM-NH$_2$ and NIR fluorescence was almost completely suppressed, demonstrating the specificity of the sensor (Figure 8b).
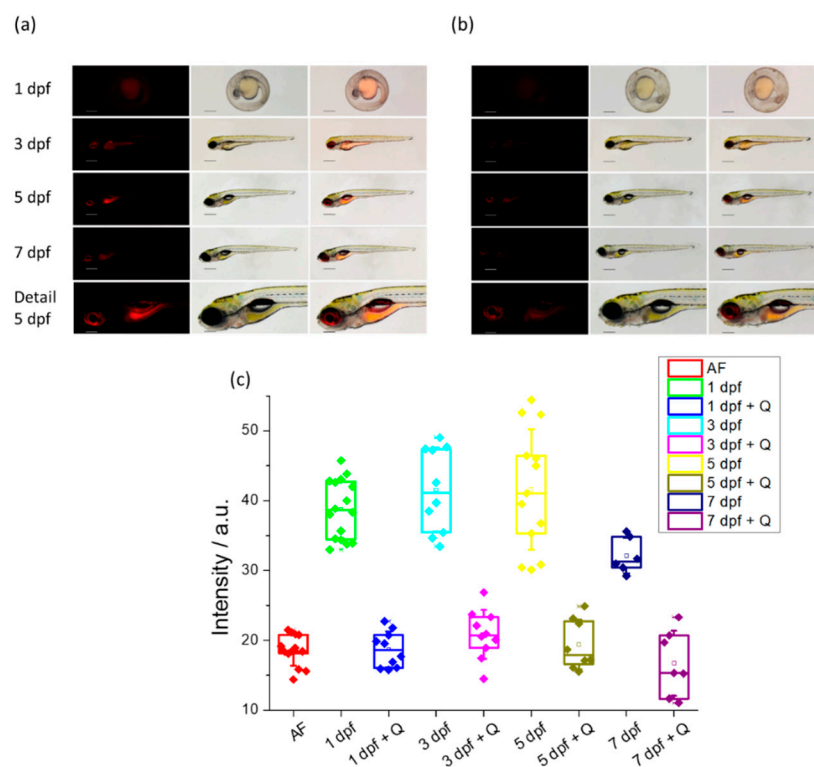

Figure 8. (**a**) Living zebrafish embryos and larvae incubated with DCM-HBU (10 μM) for 3 h at different developmental stages (1, 3, 5, and 7 dpf); red fluorescent (left), brightfield (centre), and merge (right) images were taken by a stereo microscope (λ_{ex} = 458 nm, λ_{em} = 680 nm). Detail (head with central nervous system) of a living zebrafish larva at 5 dpf is also shown. Scale bars: 1 dpf: 250 μm, 3–7 dpf: 500 μm, detail: 200 μm. (**b**) Living zebrafish embryos and larvae at the same dpf preincubated for 3 h with 200 μM quercetin and incubated with 10 μM DCM-HBU for 3 h. (**c**) Intensity values of NIR emission of zebrafish at different dpf, incubated with 10 μM DCM-HBU in presence or absence of the inhibitor quercetin. Boxes represent the 25th, 50th, and 75th percentiles. Whiskers represent the SE.

Additionally, a quantitative analysis of NIR emission was carried out. The amount of the fluorescent signal obtained after incubation with 10 μM DCM-HBU is similar during all larval time points studied (1 dpf, 3 dpf, and 5 dpf), with the exception of a slightly

smaller difference observed in 7-day-old zebrafish, when compared to the autofluorescence control. Quercetin inhibition leads to a strong reduction of the fluorescent signal down to autofluorescence levels or below (day 7). Importantly, the fluorescent signal differences between the experimental and the quercetin-inhibited conditions are similar at all time points. This suggests that the levels of enzyme available at different stages of animal development are virtually identical to each other (see Figure 8c).

4. Discussion

The design strategy of the DCM-HBU probe consisted of reacting the amine group of the 4-hydroxybenzylamine with the amine of DCM-NH$_2$, disrupting the internal charge transfer complex (ICT) that confers the spectral properties of DCM-NH$_2$ and shifting its absorption and emission spectra towards shorter wavelengths due to the electron withdrawal effect of the amide bond. Consequently, the catalytic action of TYR restored the ICT in the DCM-NH$_2$ molecule, leading to a remarkable ratiometric fluorescence between the peaks of the DCM-NH$_2$ and DCM-HBU bands. Thus, by assembling the HBU enzyme recognition cluster on the DCM-NH$_2$ fluorophore, we synthesized an extremely specific TYR fluorescent substrate. Based on the existing bibliography [37] and with the experimental results obtained, it was possible to establish the mechanism by which the enzymatic catalysis of the DCM-HBU probe substrate occurs. By the action of TYR, the probe is hydroxylated, followed by enzymatic oxidation to orthoquinone, which after a rapid intramolecular electronic rearrangement, initiates the cleavage of quinone, as indicated in Scheme 2. The IR spectrum of the reaction sample supports the proposed reaction mechanism since it shows a new band at 1680 cm^{-1} in the C=O region that is consistent with the appearance of the ketone in the proposed mechanism.

The release of the recognition group allows the typical ICT of the DCM-NH$_2$ fluorophore to be restored, resulting in NIR emission spectrum that generates the possibility of collecting a ratiometric fluorescence signal between the green fluorescence intensity of the probe and the NIR DCM-NH$_2$ fluorescence.

As TYR activity has an important interest in diagnosis and biomedical research, we study the application of the DCM-HBU probe in cells. Since melanoma is one of the medical issues with anomalous TYR activity, we selected MEL1 and A-375 cell lines as in vitro melanoma models to perform live cell studies. Once the probe has been added, both cell lines showed an increase in the R:G ratio value over time. As the initial rate of this increase is dependent on TYR activity, the measure of the slope in the initial stage can be used to determine the activity of the enzymatic reaction. From a comparative study between both cell lines, we detected a higher TYR activity in the MEL1 primary cell line than in A-375. On the other hand, the ratiometric R:G values from MEL1 melanoma cells plotted in Figure 5b as a function of time for cells without quercetin inhibitor and another one exposed to the inhibitor, show a large increase in the R:G ratio when the inhibitor is not present, while in the presence of quercetin, the increase in the R:G ratio is negligible. All these results clearly show that the probe is sensitive to the action of TYR and when this enzyme is inhibited, the substrate does not suffer alteration in its photophysical properties. Moreover, our results show that both the substrate and DCM-NH$_2$ can be excited by one green photon or two NIR photons. In both experiments, we found a measurable increase in the ratio values that is useful in the determination of TYR activity in cells through fluorescence microscopy. Excitation by NIR radiation was widely used to prevent or reduce autofluorescence of cells and tissues, as well as the absorption and scattering of excitation light, which allows obtaining sharper images at greater depths, although its use is limited in the range of wavelength of higher transmittance in biological samples [15].

Two-photon excitation microscopy is a technique of special importance in the measurement of highly scattering samples, as happens in biological tissues, firstly because NIR wavelengths scatter less than blue/green light, secondly, because there is lack of absorption outside the focus, and thirdly, two-photon excitation prevents or reduces autofluorescence of biological samples. Two-photon excitation is especially relevant for imaging of structures

that extend into the specimen, for avoiding UV excitation, for in vivo measurements or when a localized photochemistry is important [52]. All these features encouraged us to apply it to fluorescence imaging of tumour tissues at different depths. Our data allowed us to reconstruct 3D ratiometric images after two-photon excitation and the results in Figure 7b show the ratio value at a different depth measured at every incubation time. That demonstrates the potential use of this probe in biological tissues under two-photon excitation. Comparing the top and bottom slice of the tissues in the 3D images (Figure S19), it is possible to observe a higher ratio value in the upper plane than in the lower one. This could be due to a faster penetration in this level. Therefore, the probe should cross the whole tissue to reach the lower plane.

From the high levels of NIR fluorescence obtained in zebrafish larvae at different dpf incubated with the DCM-HBU probe, enzymatic TYR is predicted to be active in the yolk sac, eye, CNS, and inner organs. In addition, the quantification of the intensity of emission NIR in the recovered images from the incubation with DCM-HBU + quercetin showed only basic levels of autofluorescence, indicating that quercetin inhibits TYR activity in whole organisms. The use of this fluorescent probe, together with the imaging techniques, allow us to measure TYR activity in vivo in zebrafish. Our results suggest a similar activity during the first seven dpfs, that is, during all early developmental stages.

5. Conclusions

By the assembly of the enzyme-recognizing group 4-hydroxybenzylamine on the fluorophore dicyanomethylene-4H-pyran derivative, we synthesized the corresponding amide to obtain DCM-HBU, a TYR-sensitive and highly specific fluorescent substrate. After a TYR-mediated oxidation followed by hydrolysis of the urea linkage, the donor–acceptor DCM-NH$_2$ system is restored, showing the NIR characteristic ICT emission spectrum along with a large Stokes shift, which allows us to obtain a ratiometric fluorescence output between the green fluorescent signal of the substrate and the NIR signal of DCM-NH$_2$. In addition, both the substrate and probe are capable of being excited by two NIR photons, which made it possible to eliminate the green and red bands of autofluorescence. Owing to the possibility of being excited by two simultaneous photons, the applicability of this new probe as an intracellular in vivo sensor of TYR, as well as its ability to obtain clear fluorescence microscopy images of tumor tissues, was confirmed. Finally, the probe is useful for the quantitative sensing of TYR activity in vivo, as demonstrated in zebrafish larvae at different stages. This new two-photon ratiometric NIR fluorescent probe is expected to be useful for the accurate detection of TYR in complex biosystems at greater depths than other one-photon excited fluorescent probes.

Supplementary Materials: The following supporting information can be downloaded at: https://www.mdpi.com/article/10.3390/chemosensors11020145/s1, Figure S1: representative ICT-based two-photon excitable molecules; Synthesis of compound DCM-HBU; Scheme S1: synthesis of compound DCM-NH$_2$; Mass and NMR spectra; IR spectrum; Figure S2: absorption spectra of the DCM-HBU at different concentrations; Figure S3: molar absorptivity coefficient calculation; Figure S4: emission spectra of DCM-HBU at different concentrations; Figure S5: absorption spectrum of DCM-NH$_2$; Figure S6: emission spectra of DCM-NH$_2$; Quantum yield calculation; Table S1: fluorescence quantum yields, absorptivity coefficients and Stokes shift of DCM-NH$_2$; Figure S7: fluorescence decays of DCM-NH$_2$ and DCM-HBU; Figure S8: pH dependence of DCM-NH$_2$; Figure S9: photobleaching assay; Figure S10: evolution of the emission spectra of DCM−HBU with TYR; Figure S11: influence of pH and temperature on enzyme activity; Figure S12: IR spectra; Figure S13: two-photon excitation spectra; Figure S14: logarithmic plot of the power dependence of the relative two-photon intensity; Figure S15: representative images of the green and red intensity channels and R:G ratio images of A-375 and MEL1 cells after adding DCM-HBU; Figure S16: increase in the value of the ratio versus time of the images of MEL1 and A-375 cells; Figure S17: representative images of the green and red intensity channels of A-375 tumours after adding DCM-HBU using two-photon microscopy; Figure S18: 3D red and green intensity images of A-375 tumours after adding DCM-HBU using two-photon microscopy; Figure S19: top and bottom planes of 3D ratiometric images; Figure S20: images

of living zebrafish embryos and larvae incubated with DMSO; Video S1: fluorescence microscopy R:G ratio maps of live A-375 cell line after adding DCM-HBU and representation of the R:G ratio values over time, by two-photon excitation; Video S2: 3D ratiometric images of A-375 tumours.

Institutional Review Board Statement: The animal study protocol was revised by the Institutional Ethics Committee of the University of Granada and approved by Regional Andalusian Government, protocol code 07/07/2022/104, from 11 July 2022.

Data Availability Statement: Not Applicable.

Conflicts of Interest: The authors declare no conflict of interest. The funders had no role in the design of the study; in the collection, analyses, or interpretation of data; in the writing of the manuscript, or in the decision to publish the results.

References

1. Razgulin, A.; Ma, N.; Rao, J.H. Strategies for in vivo imaging of enzyme activity: An overview and recent advances. *Chem. Soc. Rev.* **2011**, *40*, 4186–4216. [CrossRef]
2. Wu, X.F.; Shi, W.; Li, X.H.; Ma, H.M. Recognition moieties of small molecular fluorescent probes for bioimaging of enzymes. *Acc. Chem. Res.* **2019**, *52*, 1892–1904. [CrossRef]
3. Zhang, J.J.; Chai, X.Z.; He, X.P.; Kim, H.J.; Yoon, J.; Tian, H. Fluorogenic probes for disease-relevant enzymes. *Chem. Soc. Rev.* **2019**, *48*, 683–722. [CrossRef]
4. Singh, H.; Tiwari, K.; Tiwari, R.; Pramanik, S.K.; Das, A. Small molecule as fluorescent probes for monitoring intracellular enzymatic transformations. *Chem. Rev.* **2019**, *119*, 11718–11760. [CrossRef]
5. Li, G.L.; Fu, H.L.; Chen, X.J.; Gong, P.W.; Chen, G.; Xia, L.; Wang, H.; You, J.M.; Wu, Y.N. Facile and sensitive fluorescence sensing of alkaline phosphatase activity with photoluminescent carbon dots based on inner filter effect. *Anal. Chem.* **2016**, *88*, 2720–2726. [CrossRef]
6. Zhao, J.; Ma, T.; Chang, B.; Fang, J. Recent Progress on NIR Fluorescent Probes for Enzymes. *Molecules* **2022**, *27*, 5922. [CrossRef]
7. Cao, S.P.; Pei, Z.C.; Xu, Y.Q.; Pei, Y.X. Glyco-nanovesicles with activatable near-infrared probes for real-time monitoring of drug release and targeted delivery. *Chem. Mater.* **2016**, *28*, 4501–4506. [CrossRef]
8. Li, H.D.; Yao, Q.C.; Xu, F.; Li, Y.Q.; Kim, D.Y.; Chung, J.W.; Baek, G.; Wu, X.F.; Hillman, P.F.; Lee, E.Y.; et al. An activatable aiegen probe for high-fidelity monitoring of overexpressed tumor enzyme activity and its application to surgical tumor excision. *Angew. Chem. Int. Ed.* **2020**, *59*, 10186–10195. [CrossRef]
9. Noh, C.K.; Lim, C.S.; Lee, G.H.; Cho, M.K.; Lee, H.W.; Roh, J.; Kim, Y.B.; Lee, E.; Park, B.; Kim, H.M.; et al. A diagnostic method for gastric cancer using two-photon microscopy with enzyme-selective fluorescent probes: A pilot study. *Front. Oncol.* **2021**, *11*, 634219. [CrossRef]
10. Kobayashi, H.; Ogawa, M.; Alford, R.; Choyke, P.L.; Urano, Y. New strategies for fluorescent probe design in medical diagnostic imaging. *Chem. Rev.* **2010**, *110*, 2620–2640. [CrossRef]
11. Yezhelyev, M.V.; Gao, X.; Xing, Y.; Al-Hajj, A.; Nie, S.M.; O'Regan, R.M. Emerging use of nanoparticles in diagnosis and treatment of breast cancer. *Lancet Oncol.* **2006**, *7*, 657–667. [CrossRef]
12. Diaspro, A.; Bianchini, P.; Vicidomini, G.; Faretta, M.; Ramoino, P.; Usai, C. Multi-photon excitation microscopy. *Biomed. Eng. Online* **2006**, *5*, 1–14. [CrossRef]

13. Juvekar, V.; Lee, H.W.; Kim, H.M. Two-photon fluorescent probes for detecting enzyme activities in live tissues. *ACS Appl. Bio Mater.* **2021**, *4*, 2957–2973. [CrossRef]

14. Liu, H.W.; Liu, Y.C.; Wang, P.; Zhang, X.B. Molecular engineering of two-photon fluorescent probes for bioimaging applications. *Methods Appl. Fluoresc.* **2017**, *5*, 012003. [CrossRef]

15. Shaw, P.A.; Forsyth, E.; Haseeb, F.; Yang, S.; Bradley, M.; Klausen, M. Two-photon absorption: An open door to the nir-ii biological window? *Front. Chem.* **2022**, *10*, 921354. [CrossRef]

16. Göppert-Mayer, M. Über elementarakte mit zwei quantensprüngen. *Ann. Phys.* **1931**, *401*, 273–294. [CrossRef]

17. Denk, W.; Strickler, J.; Webb, W. Two-photon laser scanning fluorescence microscopy. *Science* **1990**, *248*, 73–76. [CrossRef]

18. Ragan, T.; Kadiri, L.R.; Venkataraju, K.U.; Bahlmann, K.; Sutin, J.; Taranda, J.; Arganda-Carreras, I.; Kim, Y.; Seung, H.S.; Osten, P. Serial two-photon tomography for automated ex vivo mouse brain imaging. *Nat. Methods* **2012**, *9*, 255–258. [CrossRef]

19. Abeywickrama, C.S.; Wijesinghe, K.J.; Plescia, C.B.; Fisher, L.S.; Goodson, T.; Stahelin, R.V.; Pang, Y. A pyrene-based two-photon excitable fluorescent probe to visualize nuclei in live cells. *Photochem. Photobiol. Sci.* **2020**, *19*, 1152–1159. [CrossRef]

20. Ye, X.X.; Xiang, Y.H.; Wang, Q.R.; Li, Z.; Liu, Z.H. A red emissive two-photon fluorescence probe based on carbon dots for intracellular ph detection. *Small* **2019**, *15*, 1901673. [CrossRef]

21. Yan, M.; Fang, H.X.; Wang, X.Q.; Xu, J.J.; Zhang, C.W.; Xu, L.; Li, L. A two-photon fluorescent probe for visualizing endoplasmic reticulum peroxynitrite in parkinson's disease models. *Sens. Actuators B Chem.* **2021**, *328*, 129003. [CrossRef]

22. Zou, Y.X.; Li, M.S.; Xing, Y.L.; Duan, T.T.; Zhou, X.J.; Yu, F.B. Bioimaging of glutathione with a two-photon fluorescent probe and its potential application for surgery guide in laryngeal cancer. *ACS Sens.* **2020**, *5*, 242–249. [CrossRef]

23. Gui, R.J.; Jin, H.; Bu, X.N.; Fu, Y.X.; Wang, Z.H.; Liu, Q.Y. Recent advances in dual-emission ratiometric fluorescence probes for chemo/biosensing and bioimaging of biomarkers. *Coord. Chem. Rev.* **2019**, *383*, 82–103. [CrossRef]

24. Lee, M.H.; Kim, J.S.; Sessler, J.L. Small molecule-based ratiometric fluorescence probes for cations, anions, and biomolecules. *Chem. Soc. Rev.* **2015**, *44*, 4185–4191. [CrossRef]

25. Park, S.H.; Kwon, N.; Lee, J.H.; Yoon, J.; Shin, I. Synthetic ratiometric fluorescent probes for detection of ions. *Chem. Soc. Rev.* **2020**, *49*, 143–179. [CrossRef]

26. Jin, H.; Yang, M.; Sun, Z.J.; Gui, R.J. Ratiometric two-photon fluorescence probes for sensing, imaging and biomedicine applications at living cell and small animal levels. *Coord. Chem. Rev.* **2021**, *446*, 214114. [CrossRef]

27. Decker, H.; Schweikardt, T.; Tuczek, F. The first crystal structure of tyrosinase: All questions answered? *Angew. Chem. Int. Ed.* **2006**, *45*, 4546–4550. [CrossRef]

28. Solem, E.; Tuczek, F.; Decker, H. Tyrosinase versus catechol oxidase: One asparagine makes the difference. *Angew. Chem. Int. Ed.* **2016**, *55*, 2884–2888. [CrossRef]

29. Artes, F.; Castaner, M.; Gil, M.I. Review: Enzymatic browning in minimally processed fruit and vegetables. *Food Sci. Technol. Int.* **1998**, *4*, 377–389. [CrossRef]

30. Qu, Y.W.; Zhan, Q.; Du, S.B.; Ding, Y.; Fang, B.; Du, W.; Wu, Q.; Yu, H.D.; Li, L.; Huang, W. Catalysis-based specific detection and inhibition of tyrosinase and their application. *J. Pharm. Anal.* **2020**, *10*, 414–425. [CrossRef]

31. Espin, J.C.; Morales, M.; Varon, R.; Tudela, J.; Garciacanovas, F. A continuous spectrophotometric method for determining the monophenolase and diphenolase activities of apple polyphenol oxidase. *Anal. Biochem.* **1995**, *231*, 237–246. [CrossRef] [PubMed]

32. Li, D.; Gill, R.; Freeman, R.; Willner, I. Probing of enzyme reactions by the biocatalyst-induced association or dissociation of redox labels linked to monolayer-functionalized electrodes. *Chem. Commun.* **2006**, *48*, 5027–5029. [CrossRef] [PubMed]

33. Yildiz, H.B.; Freeman, R.; Gill, R.; Willner, I. Electrochemical, photoelectrochemical, and piezoelectric analysis of tyrosinase activity by functionalized nanoparticles. *Anal. Chem.* **2008**, *80*, 2811–2816. [CrossRef] [PubMed]

34. Gill, R.; Freeman, R.; Xu, J.P.; Willner, I.; Winograd, S.; Shweky, I.; Banin, U. Probing biocatalytic transformations with cdse-zns qds. *J. Am. Chem. Soc.* **2006**, *128*, 15376–15377. [CrossRef] [PubMed]

35. Feng, X.L.; Feng, F.D.; Yu, M.H.; He, F.; Xu, Q.L.; Tang, H.W.; Wang, S.; Li, Y.L.; Zhu, D.B. Synthesis of a new water-soluble oligo(phenylenevinylene) containing a tyrosine moiety for tyrosinase activity detection. *Org. Lett.* **2008**, *10*, 5369–5372. [CrossRef]

36. Li, X.H.; Shi, W.; Chen, S.M.; Jia, J.; Ma, H.M.; Wolfbeis, O.S. A near-infrared fluorescent probe for monitoring tyrosinase activity. *Chem. Commun.* **2010**, *46*, 2560–2562. [CrossRef]

37. Wu, X.F.; Li, L.H.; Shi, W.; Gong, Q.Y.; Ma, H.M. Near-infrared fluorescent probe with new recognition moiety for specific detection of tyrosinase activity: Design, synthesis, and application in living cells and zebrafish. *Angew. Chem. Int. Ed.* **2016**, *55*, 14728–14732. [CrossRef]

38. Wu, L.L.; Liu, J.H.; Li, P.; Tang, B.; James, T.D. Two-photon small-molecule fluorescence-based agents for sensing, imaging, and therapy within biological systems. *Chem. Soc. Rev.* **2021**, *50*, 702–734. [CrossRef]

39. Dumat, B.; Bordeau, G.; Aranda, A.I.; Mahuteau-Betzer, F.; El Harfouch, Y.; Metge, G.; Charra, F.; Fiorini-Debuisschert, C.; Teulade-Fichou, M.P. Vinyl-triphenylamine dyes, a new family of switchable fluorescent probes for targeted two-photon cellular imaging: From DNA to protein labeling. *Org. Biomol. Chem.* **2012**, *10*, 6054–6061. [CrossRef]

40. Feng, Y.C.; Cai, Z.B.; Li, S.L.; Chen, L.J.; Ye, Q.; Tian, Y.P. Novel v-shaped d-n-a-n-d two-photon absorption compounds with large stokes shifts: Synthesis, optical properties, selective detection of cysteine, and imaging in living cells. *Dye. Pigment.* **2023**, *210*, 111021. [CrossRef]

41. Abeywickrama, C.S. Large stokes shift benzothiazolium cyanine dyes with improved intramolecular charge transfer (ict) for cell imaging applications. *Chem. Commun.* **2022**, *58*, 9855–9869. [CrossRef] [PubMed]

42. Guo, Z.Q.; Zhu, W.H.; Tian, H. Dicyanomethylene-4h-pyran chromophores for oled emitters, logic gates and optical chemosensors. *Chem. Commun.* **2012**, *48*, 6073–6084. [CrossRef] [PubMed]

43. Hou, T.T.; Cai, Y.; Zhang, Z.Y.; Wang, C.Y.; Tang, Y.H.; Zhu, M.Q.; Wang, Y.L. Progress of dicyanomethylene-4h-pyran derivatives in biological sensing based on ict effect. *Front. Chem.* **2022**, *10*, 1–5. [CrossRef] [PubMed]

44. Valverde-Pozo, J.; Paredes, J.M.; Salto-Giron, C.; Herrero-Foncubierta, P.; Giron, M.D.; Miguel, D.; Cuerva, J.M.; Alvarez-Pez, J.M.; Salto, R.; Talavera, E.M. Detection by fluorescence microscopy of n-aminopeptidases in bacteria using an ict sensor with multiphoton excitation: Usefulness for super-resolution microscopy. *Sens. Actuators B Chem.* **2020**, *321*, 128487. [CrossRef]

45. Schindelin, J.; Arganda-Carreras, I.; Frise, E.; Kaynig, V.; Longair, M.; Pietzsch, T.; Preibisch, S.; Rueden, C.; Saalfeld, S.; Schmid, B.; et al. Fiji: An open-source platform for biological-image analysis. *Nat. Methods* **2012**, *9*, 676–682. [CrossRef] [PubMed]

46. Sun, W.; Fan, J.L.; Hu, C.; Cao, J.F.; Zhang, H.; Xiong, X.Q.; Wang, J.Y.; Cui, S.; Sun, S.G.; Peng, X.J. A two-photon fluorescent probe with near-infrared emission for hydrogen sulfide imaging in biosystems. *Chem. Commun.* **2013**, *49*, 3890–3892. [CrossRef]

47. Meyer, M.; Mialocq, J.C. Ground-state and single excited-state of laser-dye dcm -dipole-moments and solvent induced spectral shifts. *Opt. Commun.* **1987**, *64*, 264–268. [CrossRef]

48. Meyer, M.; Mialocq, J.C.; Rougée, M. Fluorescence lifetime measurements of the two isomers of the laser dye dcm. *Chem. Phys. Lett.* **1988**, *150*, 484–490. [CrossRef]

49. Fan, M.H.; Zhang, G.W.; Hu, X.; Xu, X.M.; Gong, D.M. Quercetin as a tyrosinase inhibitor: Inhibitory activity, conformational change and mechanism. *Food Res. Int.* **2017**, *100*, 226–233. [CrossRef]

50. Chen, Q.X.; Kubo, I. Kinetics of mushroom tyrosinase inhibition by quercetin. *J. Agric. Food Chem.* **2002**, *50*, 4108–4112. [CrossRef]

51. Chao, X.J.; Qi, Y.M.; Zhang, Y.M. Highly photostable fluorescent tracker with ph-insensitivity for long-term imaging of lysosomal dynamics in live cells. *ACS Sens.* **2021**, *6*, 786–796. [CrossRef] [PubMed]

52. Ustione, A.; Piston, D.W. A simple introduction to multiphoton microscopy. *J. Microsc.* **2011**, *243*, 221–226. [CrossRef] [PubMed]